1 Performance of a self-lifting linear air contact

T A Stolarski and S P Woolliscroft
Mechanical Engineering
School of Engineering and Design
Brunel University
Uxbridge, Middlesex, UB8 3PH, UK

Abstract

An investigation into the performance of a self-levitating linear air bearing that functions on the squeeze film principle was conducted and a detailed set of results describing its floating characteristics at various operating parameters is presented. Experimentally assessed performance of the bearing was compared with performance predicted by a computer model of the bearing

Nomenclature

C_i – arbitrary value of air film thickness
e, ε - dimensional and non-dimensional amplitude of vibration
f, F - dimensional and non-dimensional film force
g - gravitational acceleration
h, H – dimensional and non-dimensional air film thickness
h_o - average air film thickness
L – bearing's length
M - mass of the bearing
p, P – dimensional and non-dimensional pressure
p_o – ambient air pressure
R - relaxation parameter
t, τ- dimensional and non-dimensional time
w_o – off-set position/preload distance
w_a – vibration amplitude
ρ - air density
σ - squeeze number
ω - angular velocity of squeeze elements/frequency

1.   Introduction

Bearings exist in most products where something is required to slide, rotate or reciprocate. They are arguably one of the most important components in mechanical devices as they enable the operation of a vast amount of products from cars, trains and aircrafts to stereos, printers and engines. Many different types of bearings exist,

each with their own advantages, however the limits of many bearing types are becoming present due to micro and nano-scale precision engineering. Computers and other electronic equipment are becoming faster and smaller. To manufacture and assemble the components required for these products, precision engineering at micro-metre level is required. To achieve the required accuracy for this, extremely low levels of friction are crucial, this also is true for applications such as laser cutting, optical scanning, lithography, coordinate measuring and digital printing.

Static friction has a major effect when nano-accurate motion is required from stationary as the friction between two surfaces is far greater when they are stationary than when in motion [1]. Therefore it is important to reduce the coefficient of friction to a minimum to accomplish nano accurate motions.

This paper reports on the performance of a new design of linear air sliding contact operating on the squeeze film principle. The new design has been realised due to certain disadvantages with current linear sliding bearings for operation at nano-accurate levels.

1.1 Squeeze film mechanism

The squeeze film principle was studied by both Stefan [2] and Reynolds [3]. It occurs when a flat surface approaches another with a viscous fluid in-between. A resistive force is created opposing the direction of motion due to the displacement of the fluid. Load-carrying capacity generation in a squeeze film action is a well established phenomenon [4] and has been utilised to create gas squeeze film bearings by oscillating one surface perpendicularly to another at frequencies in excess of 1000 Hz [5, 6, 7]. The oscillations create a thin film of air in the order of microns between the two surfaces. Lift is generated by the squeeze film air build-up, which induces a positive mean pressure due to high viscous forces.

The simple model [4], which is used here, consists of two nominally flat plates shown in figure1. Plate A is vibrating while plate B is stationary. They are separated by an air gap h. The Reynolds equation controlling pressure generation in the air gap is,

$$\frac{\partial}{\partial x}\left(\frac{h^3 \rho}{12\mu} \frac{\partial p}{\partial x} \right) + \frac{\partial}{\partial y}\left(\frac{h^3 \rho}{12\mu} \frac{\partial p}{\partial y} \right) = \frac{\partial (\rho h)}{\partial t}$$

(1)

and can be normalized into non-dimensional form,

$$\frac{\partial}{\partial X}\left(H^3 P \frac{\partial P}{\partial X}\right) + \frac{\partial}{\partial Y}\left(H^3 P \frac{\partial P}{\partial Y}\right) = \sigma \frac{\partial (PH)}{\partial \tau}$$

(2)

Assuming sinusoidal vibration for plate A,

$$h = h_0 + e \sin(\omega t)$$

(3)

where h_0 is the average film thickness and e is the amplitude. In non-dimensional form,

$$H = 1 + \varepsilon \sin(\tau)$$

(4)

The film thickness given by equation (4) is normalized using the average film thickness h_0. Time is normalized using ω, which represents dimensionless period 2π. Other non-dimensional parameters are defined as follows:

$$(x,y) = L(X,Y);$$

$$p = p_0 P ; \qquad\qquad h = h_0 H ; \qquad \tau = \omega t$$

$$\sigma = \frac{12\mu \omega L^2}{p_0 h_0^2}$$

$$\varepsilon = \frac{e}{h_0}$$

where p_0 denotes ambient pressure. Equations (2) and (4) indicate that the pressure in the squeeze film is determined by two parameters, that is σ and ε. Quantity σ is the squeeze number and ε is the non-dimensional amplitude and $0 \le \varepsilon \le 1$. Assuming isothermal conditions and constant periphery pressure equal to p_0, the only possible factor that contributes to pressure generation in the gap is the squeeze term of the right hand side of equation (2). Equations (2) and (4) can be solved numerically for pressure P. Total film force exerted on the plates is a function of time and can be calculated from,

$$F = \int_0^1 \int_0^1 (P - 1) dX dY$$

(5)

It is interesting to examine how the film force changes with the two controlling parameters σ and ε. Figure 2 shows curves obtained by solving equations (2), (4), and (5). In order to determine the relationship between the film force and the squeeze motion and its velocity, curves representing H and $dH/d\tau$ are also plotted. It is seen from figure 2 that higher squeeze number, σ, and larger amplitude, ε, generate higher peak film force. The film force varies with the squeeze motion of plate A. In a part of the period, film force is negative and in the other part positive. This oscillation indicates the dynamic nature of mechanism responsible for the generation of pressure supporting an object.

Quantities σ and ε also affect the shapes of the film force curves and the lowest position of plate A. Analysis of figures 2a-2c reveals that at a low squeeze number and low amplitude, the film force tends to be in phase with squeeze velocity rather than squeeze displacement. At high squeeze number and high amplitude, the film force tends to be in phase with squeeze displacement (see figure 2c). Now, the question is how this unsymmetrical film force is created. There are a number of ways to answer the question. Firstly, in the limit $\sigma \to \infty$, the right hand side of equation (2) suggests that PH = const so that the right hand side remains bounded. Using $P = 1$ and $H = 1$ leads to,

$$PH = 1 \qquad \text{or} \qquad P = \frac{1}{1 + \varepsilon \sin \tau}$$

Although this cannot be an exact expression for the pressure field over the interface surface, it does indicate the unsymmetrical feature of pressure in a period clearly shown in figure 3. Secondly, the unsymmetrical pressure distribution can also be deduced from the ideal gas law and equation (2) is based on it. Air density in the original equation has been replaced by pressure. Negative pressure is not possible because negative density is not permissible as $\rho = p/RT$. Therefore, $P > 0$ has to be true but there is no upper limit for pressure which depends on σ and ε. This means that a high positive pressure is physically possible.

1.2 Previous squeeze-film linear sliding contact configurations

4

Linear air bearings that operate on the squeeze film principle are a very specific topic and have been mainly studied by Yoshimoto [5]. His early work in squeeze film air bearings investigates a simple design functioning by the use of a counter-weight. This bearing operated by means of an inversed "V" shape slider, vertically vibrating from the induced motion of the counter-weight beneath. The counter-weight is oscillated through the use of piezoelectric actuator and the bearing was experimentally confirmed to support 3.92 N at piezoelectric element amplitude of 0.5 µm [5]. This early design concept may be simple to construct yet it will always lack load capacity as it requires a counter-weight to operate and therefore the load capacity has already been reduced. Another problem found with this system was that the counter weight vibrated horizontally at certain frequencies [5].

Further work conducted by Yoshimoto included the incorporation of a damping mechanism to reduce the amount of vibration travelling through to the carried object for a design of bearing similar to the previous one [6]. This study concluded that the damping mechanism does improve the motion accuracy of the carried object by reducing the transmitted vibration amplitude and that the best material for the damping mechanism was silicon rubber.

1.3 Contact configuration and objectives of the present study

The linear air bearing used in the study presented here is illustrated in figure 4. It was manufactured from aluminium and the material used for guide way was mild steel. It consists of a square structure with 12 holes and 12 slots to create 8 elastic hinges. Four piezoelectric actuators are required to operate the structure, two of which can be seen in figure 4. Piezo-actuators are glued into place at their ends with epoxy resin. The bearing has a hollow square centre consisting of 4 inner surfaces, which have been machined to obtain a smooth and flat area.

The study undertaken had the following objectives:

1.   Model and predict the bearing performance.

This involves analysing the structure of the air bearing with the help of a finite element computer package and using a finite difference code to predict the film thickness from the bearing's pressure distribution.

2.   Experimentally validate the predicted performance.

This requires operating the linear air bearing whilst measuring various parameters such as film thickness and load-carrying capacity in terms of variation of the operating frequencies, input amplitudes and induced load.

2   Bearing concept and description

2.1 Operation

A cross-section of the linear air bearing design is shown in figure 5. The geometry has been chosen to allow four faces to deform from two actuating positions. The bearing functions by elastic hinges. An offset sinusoidal wave is applied to the 4 piezoelectric actuators at a set frequency causing the structure to flex producing a normal oscillation to the guide way. The motion that this deformation describes is illustrated in figure 6. Figure 6 shows the sequence of deformations of the bearing as a pre-load is applied from an offset voltage of 150V. For the bearing to operate, an offset voltage of around 70V will be applied with a sinusoidal wave on top. The bearing will then describe a profile during a full cycle in the following sequence B, A, B, C, B. This will occur with respect to time, dependant upon the operating frequency of the sinusoidal wave subjected to the piezoelectric actuators.

Due to the oscillation of all four inner surfaces normal to the guide-way, a squeeze film is produced at each surface allowing the bearing to support loads both vertically and horizontally. This makes the bearing quite practical for some industrial applications. Whilst the bearing is in operation there are several parameters that can be varied: operational frequency, operating amplitude determined by the input signal amplitude, pre-load amplitude determined by the voltage offset, and the mass of the bearing. Each of these variables will affect pressure within the squeeze film and therefore the squeeze film thickness, which is the main performance characteristic of the bearing as this ultimately dictates the bearing's load-carrying capacity.

2.2 Bearing specification

The linear air bearing, whose performance was investigated, has a mass of 0.208 kg and is made from aircraft grade aluminium to resist fatigue. The guide-way structure consists of a hollow square shaft made from mild steel with a length of 400mm, width 30 mm, and depth 30 mm and has been surface ground to obtain a flat smooth surface. A hollow design of guide-way was chosen to aid in the installation of distance probes within the guide-ways' surfaces by allowing wires to be threaded inside. A simple frame was manufactured to hold the guide-way in place and aid levelling.

2.3 Experimental set-up

The equipment utilized for experimental testing of the linear air contact includes a signal generator, single channel amplifier, oscilloscope, capacitance operating distance probes, and a transducer amplifier for operating the probes. A schematic diagram illustrating the set up of this equipment is shown in figure 7.

The signal generator produces a sinusoidal wave to drive the actuators at a set frequency; this signal is then offset and amplified by the piezoelectric amplifier. The end result that the actuators will experience could be a signal of 2000Hz oscillating about a 70V off-set with an amplitude of 70V, for example (therefore 0 to 140 V). The actual motion that the actuators induce on the structure will then be measured by the distance probe, amplified and sent back to the oscilloscope.

A photo of the test equipment set up is shown in figure 8; the linear air bearing is located on the guide-way to the right of the picture.

The guide-way incorporates the distance probe to measure the height that the bearing levitates from its top surface during operation. The levitation height between the guide-way and inner surface of the bearing is known as the "film thickness", which represents the mean thickness of the air cushion supporting the bearing and is typically in the region of 10 μm. It is necessary to identify the thickness as a "mean" because the top surface of the bearing is constantly oscillating/flexing due to the imposed sinusoidal input signal.

The distance probe operates from 0 - 0.127 mm and has a high refresh rate to achieve a good resolution signal. The probe operates on capacitance and has been specifically

chosen opposed to an Eddy current sensor because it is not affected by temperature or electric fields and is more accurate. The oscilloscope is used to measure the film thickness via the distance probe and the input voltage via a specific "monitor" socket within the actuator amplifying unit. The distance probe's range of 0 to 127 μm is converted into an electric signal and linearly represented by a voltage of 0 – 10 V. The actuator amplifying unit's range of 0-150 V is also linearly represented and is stepped down to 0-15 V through the monitor socket for safety.

3 Modelling of linear air bearing

It was necessary to statically model the deformation of the bearing during normal operation on to prevent possible yielding and to obtain various values for later usage in a performance prediction program. Dynamic modelling of the bearing was also required so that the natural modes of vibration could be identified to predict possible resonant frequencies.

A finite difference program was written in FORTRAN code to predict the performance of the bearing. Finite element analyses were carried out in order to understand bearing's deformation. The results from the performance prediction program are compared to the experimental results.

3.1 Structural analysis

The general shape of the bearing was initially modelled, using finite element package, to distinguish its deformed characteristics. It was modelled in 2-D because it has the same cross-section throughout. The resulting geometry was a 2-D side-profile of the bearing represented by 6-nods triangular elements. Care was taken to achieve high mesh densities at stress concentrations around the elastic hinges.

3.1.1 Static deformation and profile

A displacement of 10 μm was applied to each "B line" shown in figure 9, acting outwards to simulate expansion of the actuators. This is equivalent to the excitation of

each actuator fully at 150 V therefore obtaining the maximum obtainable displacement/stroke for each of the four actuators.

The profile created by this deformation is illustrated in figure 9. The solid shape represents the outline of the structure during piezoelectric actuator excitation and the faint lines represent the shape of the structure with no excitation. The deformation of each inner surface normal to the guide-way can be seen, however this has been exaggerated in this diagram for ease of viewing as in reality this deformation would be undetectable by a naked eye. When the bearing is under operation it will deform to this shape a few thousand of times per second and thus create a squeeze film between it and the guide-way.

The finite element modelling has assumed that the piezoelectric actuators are capable of achieving their maximum stroke. This is not exactly true, as a reaction force from the bearing will restrict some of this motion; this is known as "blocked deflection" and works in accordance with figure 10. The two lines represent two different voltages of excitation, full 100% and 50%. Any position along these two lines is possible during 50% and 100% excitation depending upon the reaction force of the structure at a certain displacement. Position A represents an actuator under the influence of its maximum load and illustrates that even with 100% excitation no expansion can be achieved, whereas position B demonstrates that when the reaction force is zero, an actuator is capable of achieving its full expansion (stroke). The same applies to positions C and D but as only 50% of the excitation voltage is used only 50% of the maximum force or expansion can be achieved. Even though the full range of actuator stroke is available during the operation of the bearing it was not used for actuator safety reason. The deflection changes linearly with voltage.

3.1.2   Stress within the bearing structure

The maximum von-Mises equivalent stress for the structure was calculated to determine whether failure was likely to occur during normal operation (figure 11). The stress concentration around each of the elastic hinges is visible in a closer view in figure 12. The maximum von-Mises stress within the bearing, 40.96 MPa, can be observed within both contour plots. Similar stress concentration values will exist

around the other three inner elastic hinges as they all have the same dimensions. The maximum allowable von-Mises stress level for the material used is 73 MPa therefore operation of the bearing at full excitation voltage is acceptable as this is still well within the elastic region of the material.

3.1.3   Modal Analysis

A modal analysis of the bearing geometry was conducted to find the modal shapes and resonant frequencies. Finding the resonant frequencies of the bearing may be beneficial as operation at resonance will created larger deformations and therefore induce a larger film thickness thus increasing the load capacity. Also operation at a resonant frequency might reduce the power consumption as smaller amplitudes could be used to achieve similar film thicknesses.

To identify the resonant modes of the bearing its finite element model was constructed. The model was then subjected to a frequency range from 0-3000 Hz. This was to simulate the bearing operating for its complete achievable frequency range.

Several modal shapes were exposed during this analysis at various frequencies. However, many of them did not describe the correct motion to benefit squeeze film generation. Two possible advantageous modes are illustrated in figure 13 and figure 14: the first occurs at 2716 Hz and the second at 2511 Hz.

3.2   Film thickness prediction

A program based on the finite difference method was developed to predict the film thickness for the bearing's top inner surface. It was not necessary to predict the film thickness for the other three surfaces as they do not carry any loads but are required to stabilise the bearing's motion. The program uses various input data such as operation frequency, mass, amplitude, pre-load distance and bearing dimensions to calculate its floating height. Some assumptions were made so that the equations behind the program could be used:

(1) Squeeze film pressure is uniform in y-axis.

(2) Film thickness in uniform in z-axis.

(3) Fluid is Newtonian (air, viscosity at all shear rates remains constant).

3.2.1   Governing equations

The prediction program uses the same nonlinear parabolic partial differential Reynolds' equation that has been used in other squeeze film studies [8]. This equation governs the change in dimensionless film thickness and pressure in the x and z planes (figure 15) and can only be solved analytically for limited cases [10]. So, a numerical method, elaborated elsewhere [8], has to be employed. As finite difference method was used it required discretization where the partial derivatives are replaced with finite approximations. Dimensionless parameters, X, Y, P, H, and T are used as the equation has been normalised however the parameter Y is not included as the pressure is assumed to be constant throughout y. Thus,

$$\frac{\partial}{\partial X}\left[H^3 P \frac{\partial P}{\partial X} \right] + \frac{\partial}{\partial Z}\left[H^3 P \frac{\partial P}{\partial Z} \right] = \sigma \frac{\partial (PH)}{\partial T}$$

(6)

Where the squeeze film number is given by:

$$\sigma = \frac{12 \mu \omega L^2}{p_o h_o^2}$$

(7)

Equation (6) can be expanded, with the product rule, to give:

$$PH^3 \frac{\partial^2 P}{\partial X^2} + H^3 \left[\frac{\partial P}{\partial X} \right]^2 + 3PH^2 \frac{\partial P}{\partial X} \frac{\partial H}{\partial X} +$$
$$+ PH^3 \frac{\partial^2 P}{\partial Z^2} + H^3 \left[\frac{\partial P}{\partial Z} \right]^2 + 3PH^2 \frac{\partial P}{\partial Z} \frac{\partial H}{\partial Z} = \sigma H \frac{\partial P}{\partial T}$$

(8)

The implicit discretization can now be applied by substituting the partial derivatives for eqns (9), (10) and (11).

$$\frac{\partial P}{\partial X} = \frac{P_{i+1,j}^n - P_{i-1,j}^n}{2\Delta X}; \frac{\partial P}{\partial Z} = \frac{P_{i+1,j}^n - P_{i-1,j}^n}{2\Delta Z}; \frac{\partial H}{\partial X} = \frac{H_{i+1,j}^n - H_{i-1,j}^n}{2\Delta X}$$

(9)

$$\frac{\partial P}{\partial T} = \frac{P_{i,j}^n - P_{i,j}^{n-1}}{\Delta T}; \frac{\partial H}{\partial T} = \frac{H_{i,j}^n - H_{i,j}^{n-1}}{\Delta T}$$

(10)

$$\frac{\partial^2 P}{\partial X^2} = \frac{P_{i+1,j}^n - 2P_{i,j}^n + P_{i-1,j}^n}{\Delta X^2} ; \frac{\partial^2 P}{\partial Z^2} = \frac{P_{i+1,j}^n - 2P_{i,j}^n + P_{i-1,j}^n}{\Delta Z^2} \tag{11}$$

Substitution of the partial derivatives and rearrangement produces equation for $P_{i,j}^n$.

This is the equation used in the computer code. Other equations required include the relaxation equation (eqn 12), equation of motion (eqn 13), film thickness equation (eqns 14 and 15) and equation (16) to calculate the time average force generated from one pressure cycle.

$$P^R = [P_2 + RP(P - P_2)]^{R-1} \tag{12}$$

$$M \frac{\partial^2 y}{\partial t^2} = f - Mg \tag{13}$$

$$H = \frac{h(x,t)}{C_i} = \frac{h_o}{C_i} + \frac{2x}{C_i}[w_o + w_a \sin(\omega t)] \tag{14}$$

$$H = \frac{h(x,t)}{C_i} = \frac{h_o}{C_i} + \frac{2w_o(1-x)}{C_i}[w_o + w_a \sin(\omega t)] \tag{15}$$

$$F = \iint (P - 1) \partial X \partial Z \tag{16}$$

The physical parameters for equations (14) and (15) are illustrated in figure 16. The uppermost line indicates the position of the bearing's upper inner surface at the peak of an excitation signal and the lowest most line indicates its position at a trough. Note that equation (14) is only valid when $0 \leq x \leq \frac{1}{2}$ and equation (15) is valid only when $\frac{1}{2} \leq x \leq 1$.

3.3. Computer model results

In order to solve governing equations, a dedicated computer programme was developed. The program was used to predict the bearing's air film thicknesses at an off-set voltage of 70V, at amplitudes of 60V, 50V, 40V and 30V, with a frequency range from 500–3000Hz at intervals of 500Hz, the results are shown in figure 17. The general trend for each amplitude can be seen to increase with frequency; this was expected as a larger frequency would increase the squeeze film number, σ, leading to a larger film thickness as the viscous forces oppose the flow of air [9]. Obviously the

12

larger the input amplitude the greater the induced film thickness, this relationship is shown to be linear by the equal spacing between the lines, this is also demonstrated in other studies [5]. The prediction program shows that the bearing should be able to achieve a film thickness of almost 20 μm at 3000 Hz.

The positive mean pressure developed by the squeeze film action can be clearly seen in figure 18 by the positive volume at time step 4 (above ambient pressure indicated by P=1) being larger than the negative volume at time step 2 (below ambient pressure). The positive pressure peaks at 1.38 generate 0.38 above ambient pressure whilst the negative pressure peaks at 0.87 produce 0.13 below ambient pressure. From this graph alone it can be seen that an overall pressure generation of 0.25 above ambient pressure is possible at just one time step. The program calculates the net generated pressure over all the time steps to produce a more accurate result.

4   Experimental validation

Performance of the linear air contact was assessed experimentally in order to generate results, which could be used to validate computer model predictions and to obtain a better insight into its real operation.

4.1 Static test

The first test was to measure the pre-loaded distance with relation to voltage input (off-set) in order to obtain deformed characteristics of the bearing. This was achieved by placing the bearing directly over the distance probe on the top surface of the guide-way. Within this test a DC voltage (off-set) of 0-100 V at increments of 10 V was applied whilst recording the change in height (due to flex) for the centre of the upper bearing surface (peak point in figure 16). The bearing was then rotated through 180 degrees and the process repeated for the bottom surface to check that both surfaces were deformed in the same manner by the four piezoelectric actuators. The voltage to displacement relationship should be linear as the bearing's material is in its elastic region and because the actuators should expand linearly with applied voltage.

4. 2   Frequency tests

To fully operate the bearing and attain a squeeze film it must be subjected to an oscillation of set amplitude about its preloaded position. This is accomplished by inputting a sine-wave with an off-set voltage as previously described, for instance a wave with a mean of 70 V and amplitude of 50 V, therefore oscillating 50 V either side of 70 V. Obviously this could be conducted for any number of frequencies and amplitudes, therefore preliminary tests were conducted to determine the capabilities of the test equipment and bearing.

For all tests an offset voltage of 70 V was employed and the maximum amplitude used was 60V. The test equipment could power the 4 actuators up to 3000Hz for a reasonable range of amplitudes. Therefore a test plan of 0-3000Hz at increments of 100Hz at amplitudes of 20 V, 30 V, 40 V, 50 V, and 60 V with a fixed offset of 70 V was implemented.

To implement the proposed test plan the bearing was placed over the displacement probe in the guide-way. Then an offset voltage was applied to create the preloaded position, the frequency set and the amplitude adjusted; this caused the bearing to float. During floatation the "mean float height" and "peak to peak" oscillation value (of the bearing's top inner surface) was recorded from the oscilloscope. The amplitude was then decreased to zero and the mean height was recorded again to attain a "zero height" with no floatation. This process was repeated twice for each of the following amplitudes: 20 V, 30 V, 40 V, 50 V and 60 V to attain independent reliable results. The frequency was then increased by 100Hz and the whole process was repeated again until 3000Hz was reached.

The main parameter to be recorded during this frequency investigation was the film thickness as this dictated the bearings load capacity. It was important that both the mean float height and zero height were accurately measured as the film thickness is in the order of micrometers. This means that taking the mean film height in one position and the zero height in another would affect the results. This is why it was necessary to repeat zero height reading for each individual input amplitude as slight motion is inevitable during such low friction operation.

4. 3 Load-carrying capacity tests

The frequency that produced the largest film thickness was chosen to conduct the load-carrying capacity tests. Therefore, the load capacity was investigated at 2600Hz alone as this frequency produced the largest film thickness by far.

To study the load-carrying capacity, four small rubber mounts were installed at each corner of the top surface so that loads could be applied centrally and kept in a position . A glass dish was then installed on top of the rubber mounts and the load applied centrally on top, as shown in figure 19. The load was gradually increased with individual weights from a mass of 0 to 0.5 kg at 0.05 kg intervals. The mean float height, peak-to-peak amplitude, and zero height were recorded for excitation amplitudes of 40 V, 50 V and 60 V respectively each time a new weight was applied.

5   Results and discussion

The results produced through experimental testing, finite element modelling and the film thickness computer predictions are now presented in detail and discussed.

5.1   Experimental results

5.1.1   Static testing

The experimental results for the static tests are illustrated in figure 20 where both the top and bottom surfaces are shown together for comparison. A close linear trend for both surfaces is followed reinforcing the earlier assumption that the bearing material would be in its elastic region and that the piezoelectric actuator's stroke is linearly proportional to applied voltage. All the plots represent the displacement at the centre of the bearing's top inner surface whilst increasing and decreasing the voltage supply to the piezoelectric actuators.

5.1.2   Frequency tests

The results for all the tested amplitudes are illustrated in figure 21 and only go down to 600 Hz as no significant floatation was possible below this frequency. All results were

recorded from the frequency point where floatation began onwards for all input amplitudes, such as 900Hz for the 20 V input signal amplitude.

Each peak, in figure 21, represents a large film thickness value as the bearing is at (or close to) a resonance frequency. This is proven from the large amplitude oscillation of the bearing's surface at these frequencies illustrated in figure 22. The main resonant peak is at 2600Hz and a maximum film thickness of 20.57 μm is achieved at this point by bearing surface oscillation amplitudes of 9.97 μm. The low film thickness values below 2 μm do not represent floatation as the bearing did not experience low friction motion at these values because of surface roughness interference between the bearing and guide-way.

Figure 21 demonstrates that the input amplitude has less significance at frequencies other then resonance frequency. For instance the 20 V input amplitude barely produces a film at most frequencies yet generates 17 μm film at the main 2600Hz resonance. This fact could be used to reduce power consumption during bearing operation.

It is interesting to see that the main experimental resonant frequency occurs at 2600Hz that is nearly exactly in-between the two resonant frequencies predicted by the finite element modal analysis with one at 2511Hz and the other at 2716Hz. The slight discrepancy here could have been caused by omitting intricate details of the bearing such as the 12 steel screws holding the bearing parts together as in reality they would affect resonance as they have a greater density than the surrounding material. However including these in the finite element model would have been complex and time consuming.

The two previously mentioned graphs (figure 21 and figure 22) demonstrate the link between surface oscillation height and film thickness, either due to resonance or input amplitude. As expected, the larger the input voltage amplitude the greater the bearing surface oscillation amplitude (because the piezoelectric actuator stroke increases) and therefore the thicker the film thickness (levitation height). Resonant points also follow this trend apart from at 2500Hz where the surface oscillation amplitude for 50 V and 40 V exceed the trace for 60 V yet this is not reflected in the film thickness plot. This point should be regarded as an anomaly and may have occurred due to the inaccuracy of the signal generator during frequency adjustment for each point (±30Hz). Apart from this

anomaly most other peaks and troughs in the oscillation amplitude plot (figure 22) correlate to peaks and troughs in the film thickness plot (figure 21).

It is interesting to note that the measured bearing's surface oscillation amplitude results (figure 22) are considerably different to the measured static preload values (figure 20). According to the preload measurements an input voltage of 50 V should deform the bearing's surface 3 to 4 μm, however figure 22 illustrates that amplitudes of 3 μm to 4 μm are only present during 1200Hz to 2000Hz. At 2500Hz amplitudes of 9.5 μm are produced with the same input voltage, this clearly indicates the effect of resonance increasing the surface oscillation amplitude.

Resonance is advantageous in this bearing as it increases the film thickness yet on the other hand it may well reduce the life of the bearing by subjecting it to greater stress. If the structure is resonating in a mode with the same characteristics as the operating motion then its stress levels will be linearly proportional to the motion. Therefore as the maximum amplitude is 10 μm (figure 22) and the measured preload distance is 6.5 μm (figure 20) then the total displacement from the original position is 16.5 μm. This is roughly the same displacement value predicted by finite element model (16.3 μm) for 150 V offset voltage. Therefore the maximum stress in the bearing will be equal to 41 MPa, so the bearing should be safe to operate at 2600Hz resonance even during full input signal amplitudes as it is still in its elastic region (material yields at 73 MPa). According to calculations presuming a linear relationship to stress and that the bearing only deforms at its hinges, plastic deformation of the bearing's material should not occur until its surface has deformed beyond 29 μm, therefore amplitudes of 22.5µm should not be exceeded with an off-set voltage of 70 V.

5.1.3   Load-carrying capacity testing

Figure 23 illustrates the load capacity results; a clear trend of film thickness reduction with mass application is demonstrated. This behaviour is expected during loading as the air is compressed by the additional weight.

The obvious input amplitude trend has occurred again with larger input amplitudes sustaining a thicker film under the same load. The zero mass film thickness is smaller here than in figure 21 as it includes the mass of the rubber mounts and glass dish.

The film thickness versus applied load on the contact results have been plotted up to
0.2 kg of additional mass.

5.2   Comparison of results

5.2.1   Static tests

The experimental static pre-load test is compared with the finite element model results
in figure 24. The computing results follow a clear linear trend. The pre-load
displacement values are clearly over predicted by the model results when compared to
the experimental results as only half the predicted value is attained at some points.
This large discrepancy could be due to a larger than calculated reaction force opposing
the actuators motion thus increasing the effect of blocked deflection as described
earlier.

Another likely cause for the over-prediction of the pre-load distance from finite element
model could be due to the movement in the bearing's joints. Even though the four
components that make the bearing up are screwed together tightly, tiny amounts of
slack or play will still be present and could allow some of the piezoelectric actuator
motion to be wasted.

Whatever the real explanation for the over-prediction the disparities of the pre-load
displacement results will directly affect the performance of the film thickness prediction
program as parameters within this program are based upon computer model pre-load
displacement values.

5.2.2   Frequency performance

The comparison between the experimental and computer program predicted film
thickness results is shown in figure 25. For clarity only one experimental input
amplitude plot has been shown (60 V) along with the corresponding prediction program
plots.

A significant discrepancy between the experimental and theoretical plots can be
observed in figure 25. Even when ignoring the resonant peaks (which were not
modelled in the prediction program) the theoretical results appear to over-predict the
bearings performance for the majority of the measured frequency range. This over-

prediction of theoretical results has occurred in a previous study [7]. Here it is put down to surface finish of the squeeze film generating area and inertia effects. The over-prediction of computer model could be due to two main physical factors:

(1) hysteresis (causing the bearing to lag returning shape), and (2) quality of bearing and guide-way manufacture (mainly surface finish and squareness). Alternatively the discrepancies could be due to an error from representing the problem in the prediction program itself, such as the assumptions that atmospheric pressure is present at along the x and z axis.

6.   Conclusions

The conclusions resulting from studies presented in this paper are summarised below:

(i)   The bearing concept has been experimentally confirmed.

(ii)   Detailed set of results for the performance characteristics of the linear air bearing has   been obtained for both normal and loaded operation.

(iii)   Main resonant frequency of the bearing was found to be 2600Hz.

(iv)   Maximum load of 3.9 N was supported by the contact

(v)   It was found that squeeze film air contacts can be operated at resonance to produce extremely large amplitudes of surface oscillation, which leads to considerable film thicknesses.

It has been found that the general performance of air linear contacts, operating on the squeeze film principle is extremely sensitive to the surface finish of their squeeze film generating area. This fact alone has been concluded to be the main contributor to the broad overestimation of the prediction program at frequencies other than resonance.

7.   References

1. Stolarski, T.A., Tribology in Machine Design, Butterworth-Heinemann, 2000.
2. Dowson, D., History of tribology, New York, ASME, 1999.
3. Szeri, A.Z., Fluid film lubrication; theory and design, Cambridge University Press, 1998.
4. Stolarski, T.A. and Wei Chai, Load-carrying capacity generation in squeeze film action, Int. J. Mech. Sci., 48, 736-741, 2006.

5. Yoshimoto, S. Anno, Y. Rectangular Squeeze-Film Gas Bearing Using a Piezoelectric Actuato*r*. Japan Soc. Prec. Eng., 27, 3, 259-263, 1993.
6. Yoshimoto, S. Floating Characteristics of Squeeze-film Gas Bearings With Vibration Absorber for Linear Motion Guide. ASME. Journal of Tribology, 19, 531-535, 1997.
7. Yoshimoto, S. Anno, Y. Sato, Y. Hamanaka, K. Float Characteristics of Squeeze-Film Gas Bearing with Elastic Hinges for Linear Motion Guide. Japan Soc. Prec. Eng., 60, 574, 2109-2115, 1994.
8. Wei Chai, Performance of a linear sliding bearing operating on squeeze film principle, MPhil Thesis, Brunel University, 2003.
9. Salbu, E.O.J., Compressible squeeze films and squeeze bearings, Trans. ASME, Series D, J. Basic Eng., 86, 355-366, 1964.
10. Michael, W.A., Approximate Methods for Time-dependant Gas-film Lubrication Problems, Trans. ASME, J. Appl. Mech., 87, 509-517, 1963.

Figure Captions

Figure 1   Squeeze air film between two square plates

Figure 2   (a) Film force for ε = 0.1 and three values of the squeeze number σ equal to 10.56, 105.6, 1056; (b) film force for ε = 0.3 and three values of the squeeze number σ equal to 10.56, 105.6, 1056; (c) film
force   for ε = 0.8 and three values of the squeeze number σ equal to 10.56, 105.6, 1056.

Figure 3   Unsymmetrical pressure in a squeeze air film at infinite squeeze number, σ for ε = 0.5 and ε = 0.8.

Figure 4   Photograph showing linear squeeze film bearing with piezo-actuators attached.

Figure 5   Schematic diagram of tested linear bearing.

Figure 6   Diagram showing deformations of the linear bearing in sequence.

Figure 7   Schematic diagram of test apparatus.

Figure 8   Photograph showing test apparatus set up.

Figure 9   Exaggerated deformation of the linear bearing.

Figure 10   Piezo-electric actuator blocked deflection diagram.

Figure 11   Stress map (von Mises).

Figure 12   Close up of von Mises stress at a hinge.

Figure 13   Modal shape of the linear bearing t 2716 Hz.

Figure 14   Modal shape of the linear bearing at 2511 Hz.

Figure 15   Diagram showing discretization scheme.

Figure 16   Diagram showing parameters characterizing surface displacement.

Figure 17   Predicted film thickness as a function of frequency.

Figure 18   Pressure profile under top surface at different time steps.

Figure 19   Photograph showing linear bearing with applied load (dead weight).

Figure 20   Linear bearing deformation as a function of applied offset voltage (pre-load).

Figure 21   Film thickness as a function of frequency at offset of 70 V.

Figure 22   Oscillation amplitude as a function of frequency at offset of 70 V.

Figure 23   Film thickness as a function of applied load on the linear bearing.

Figure 24   Deformation of the linear bearing as a function of offset voltage. Comparison of experimental and computed results.

Figure 25   Film thickness as a function of frequency. Comparison of computed and experimental results.

$$h = h_0 + e \sin(\omega t)$$

Figure 1

(1) H

(2) dH/dT

(3) $\sigma = 10.56$

(4) $\sigma = 105.6$

(5) $\sigma = 1056$

Figure 2a

(1) H
(2) dH/dT
(3) σ = 10.56
(4) σ = 105.6
(5) σ = 1056

Figure 2b

(1) H
(2) dH/dT
(3) σ = 10.56
(4) σ = 105.6
(5) σ = 1056
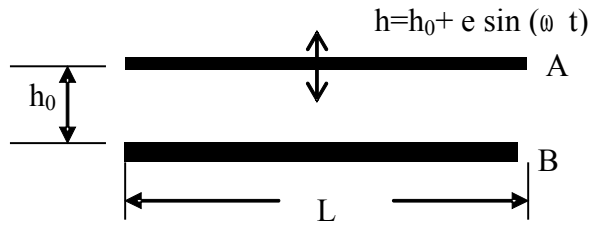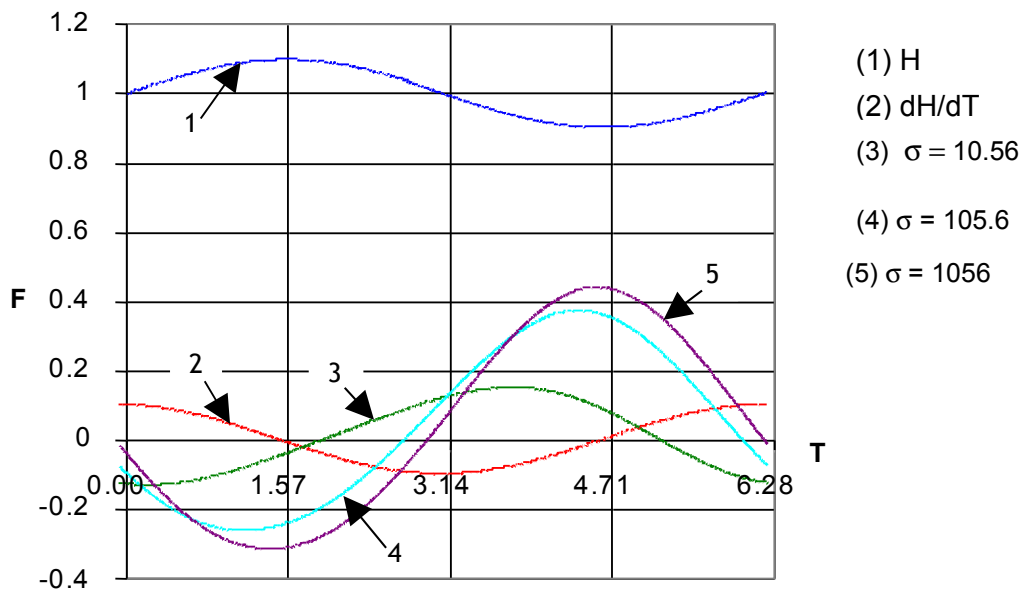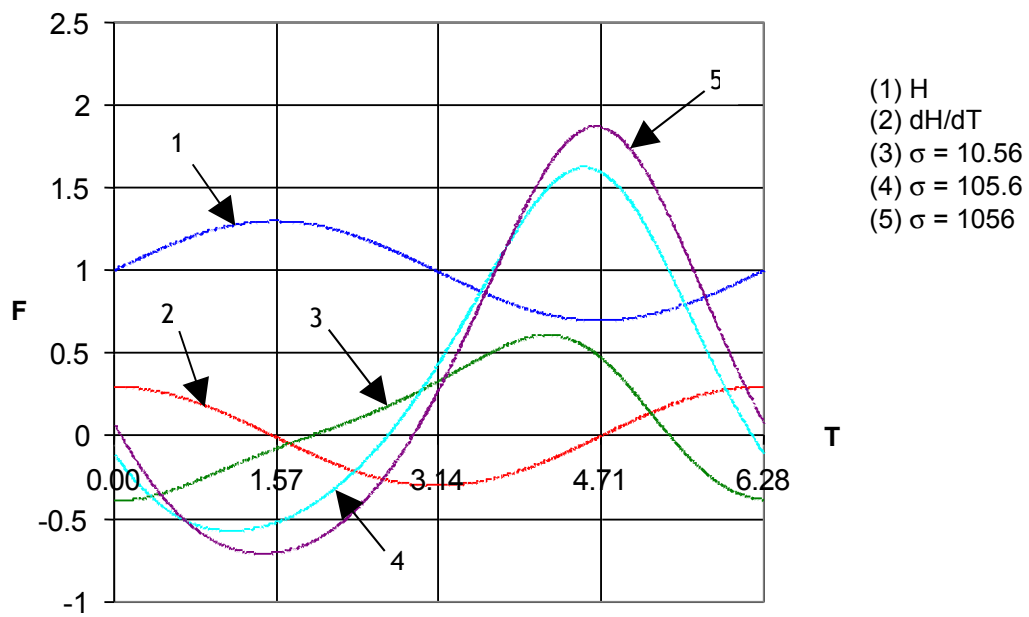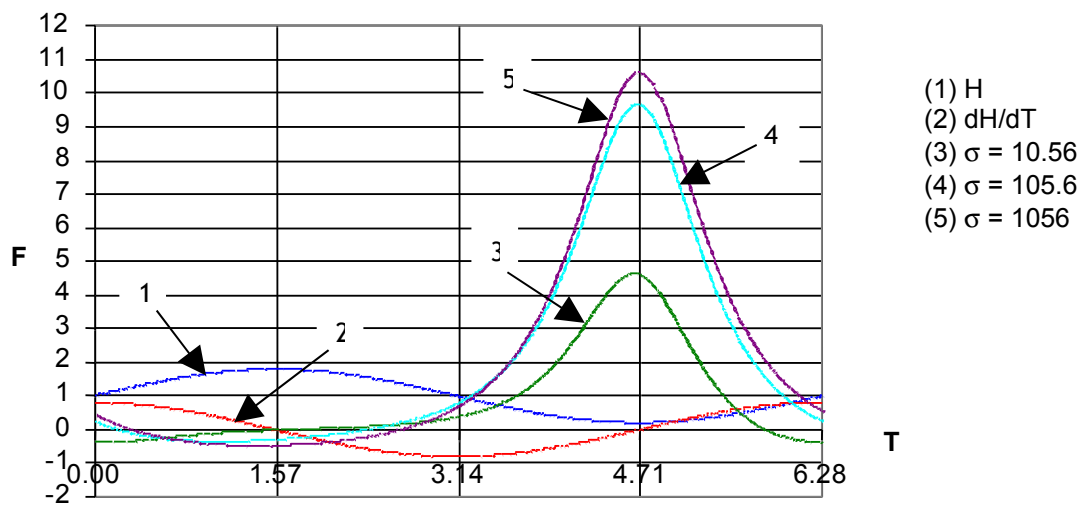
Figure 2c

Figure 3

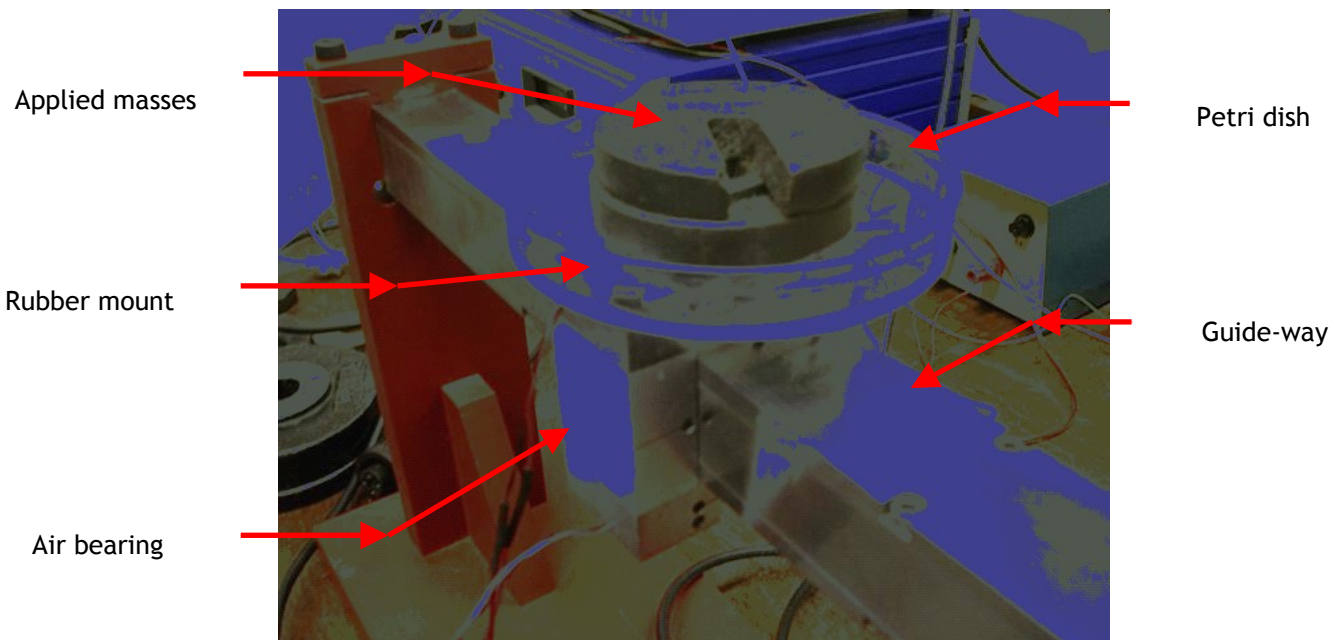Figure 4

Figure 5

Figure 6

Distance probe

Signal Generator

Piezoelectric Actuator Amplifier

Distance Probe Amplifier

Digital Oscilloscope

(Monitor Signal)

Cross-section of guide-way

Distance probe amplifier

Signal generator

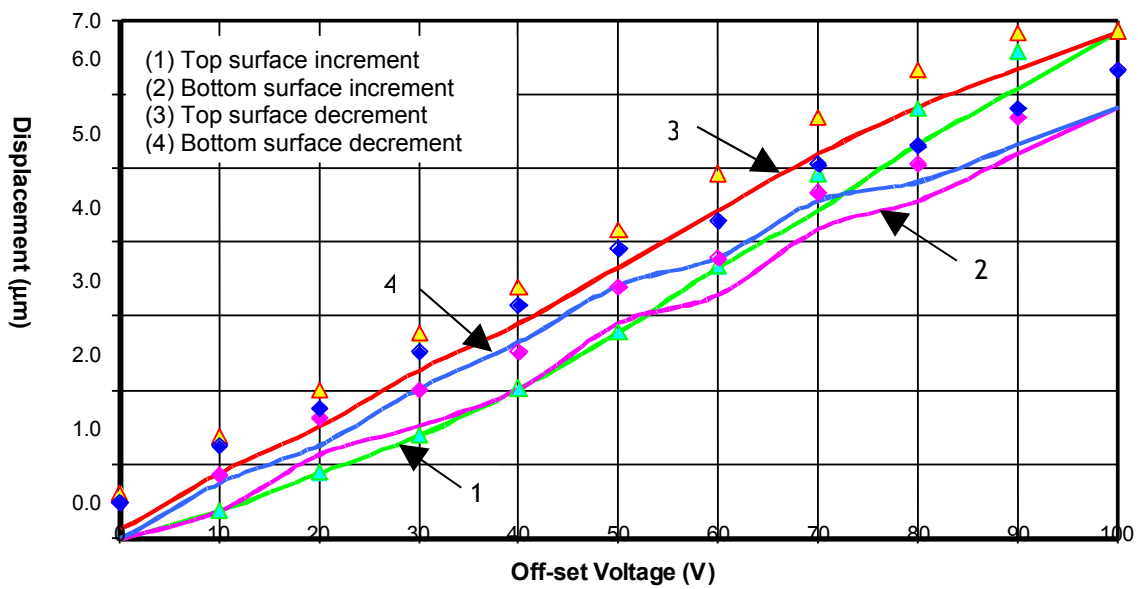Actuator amplifier

Connector

Bearing on guide-way

Guide-way

Guide-way holder
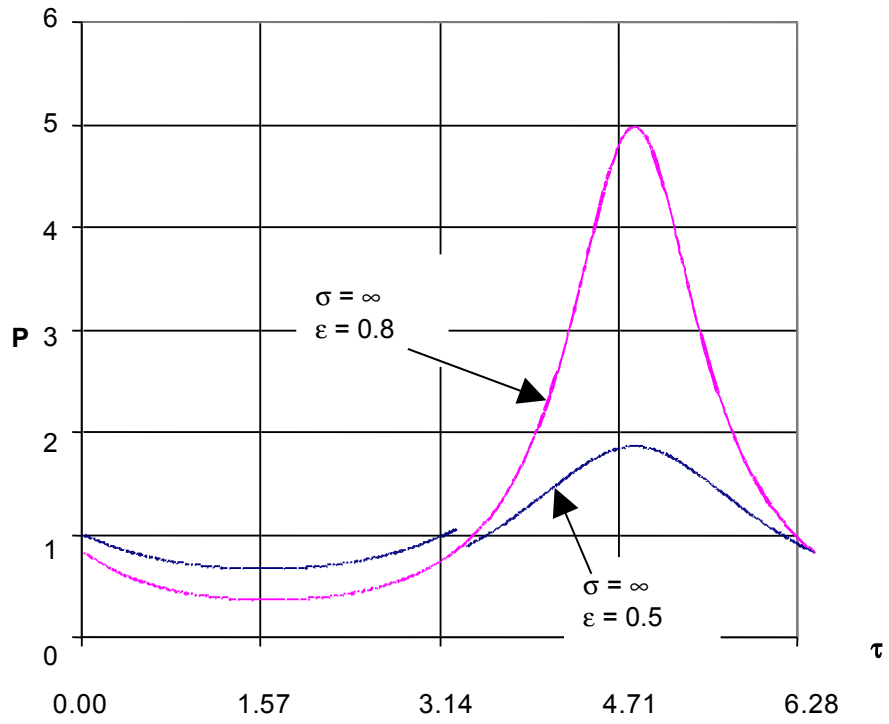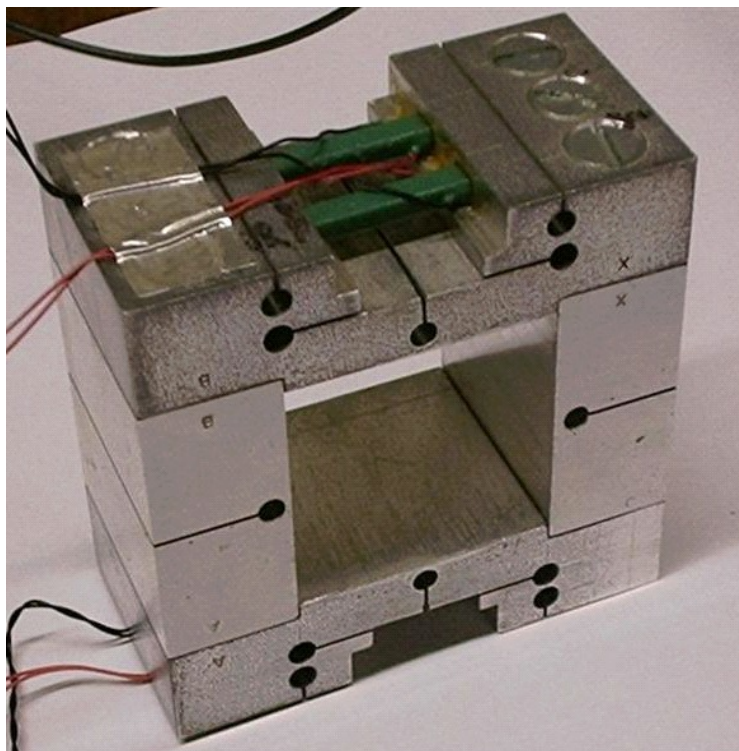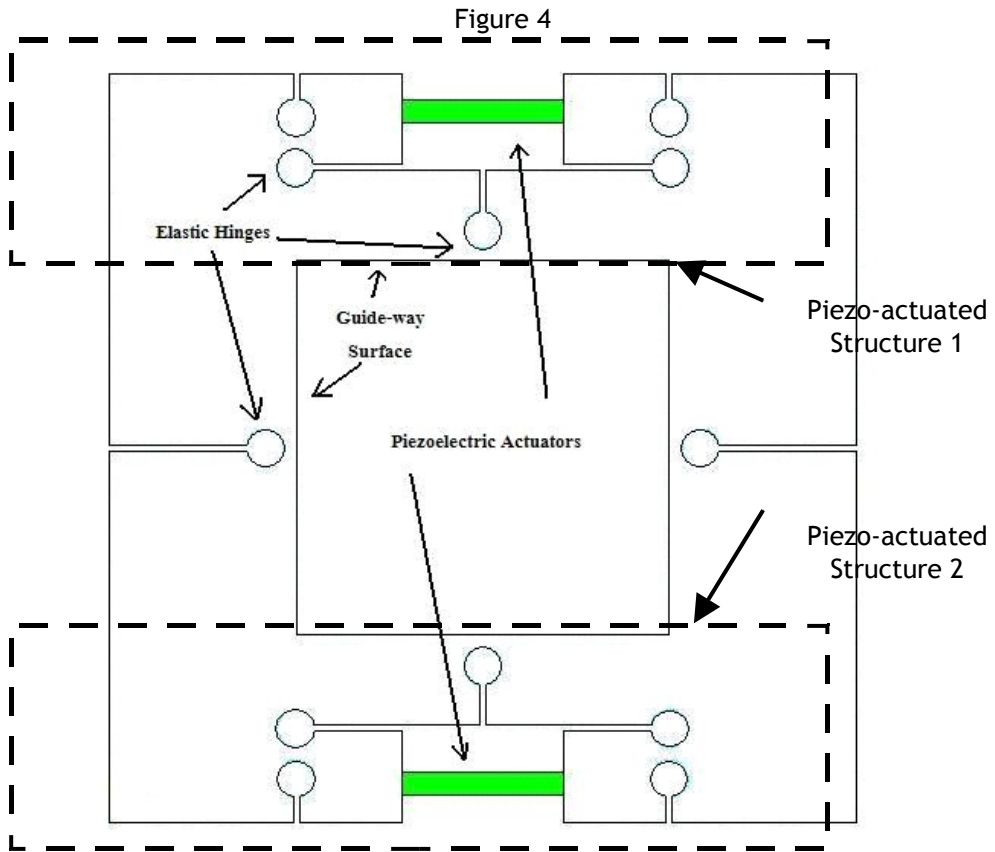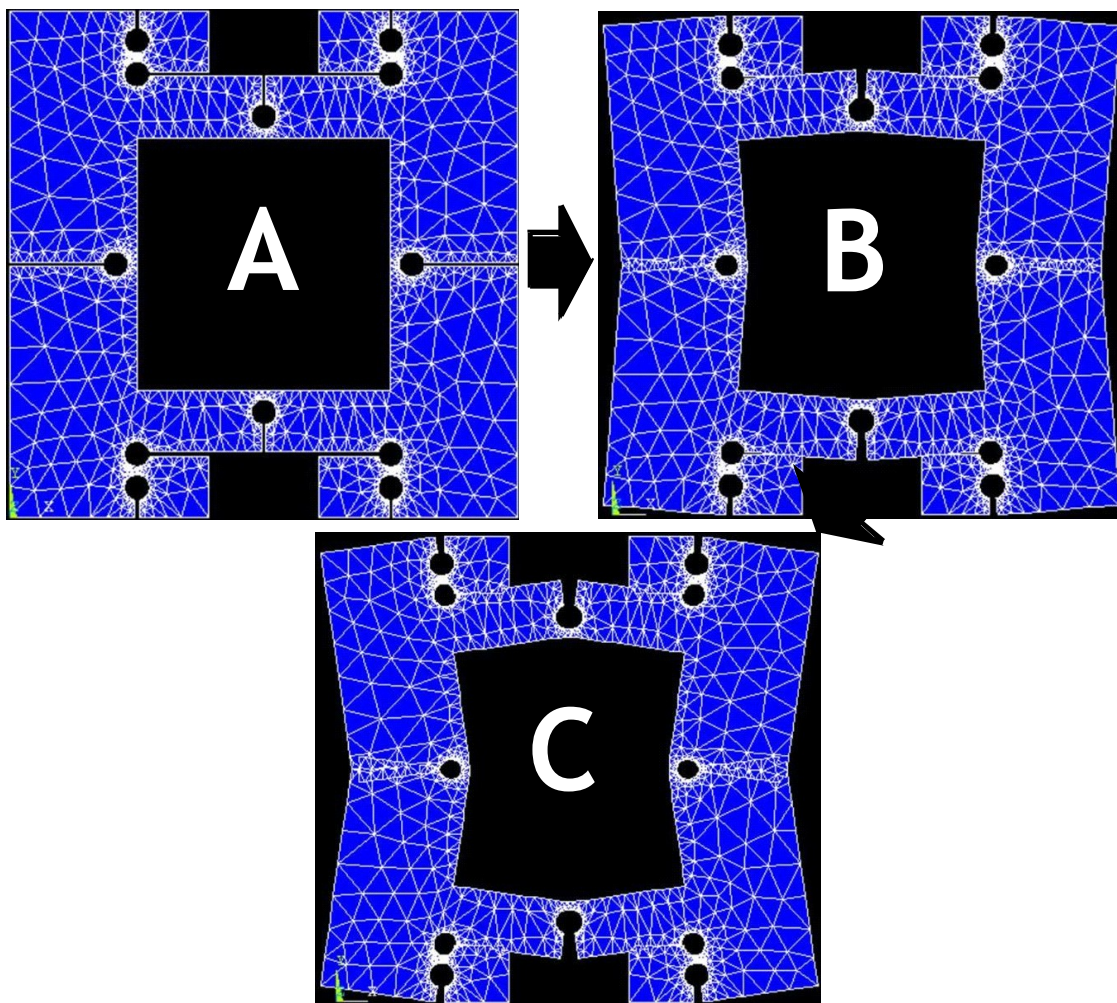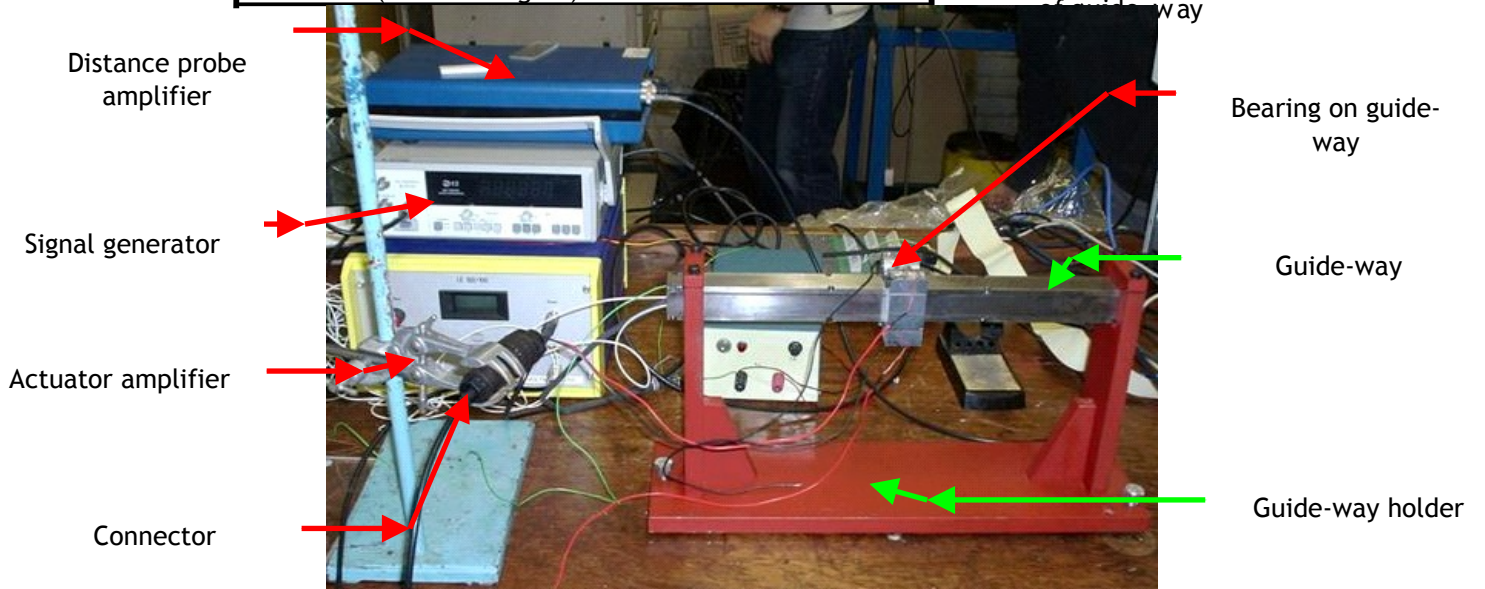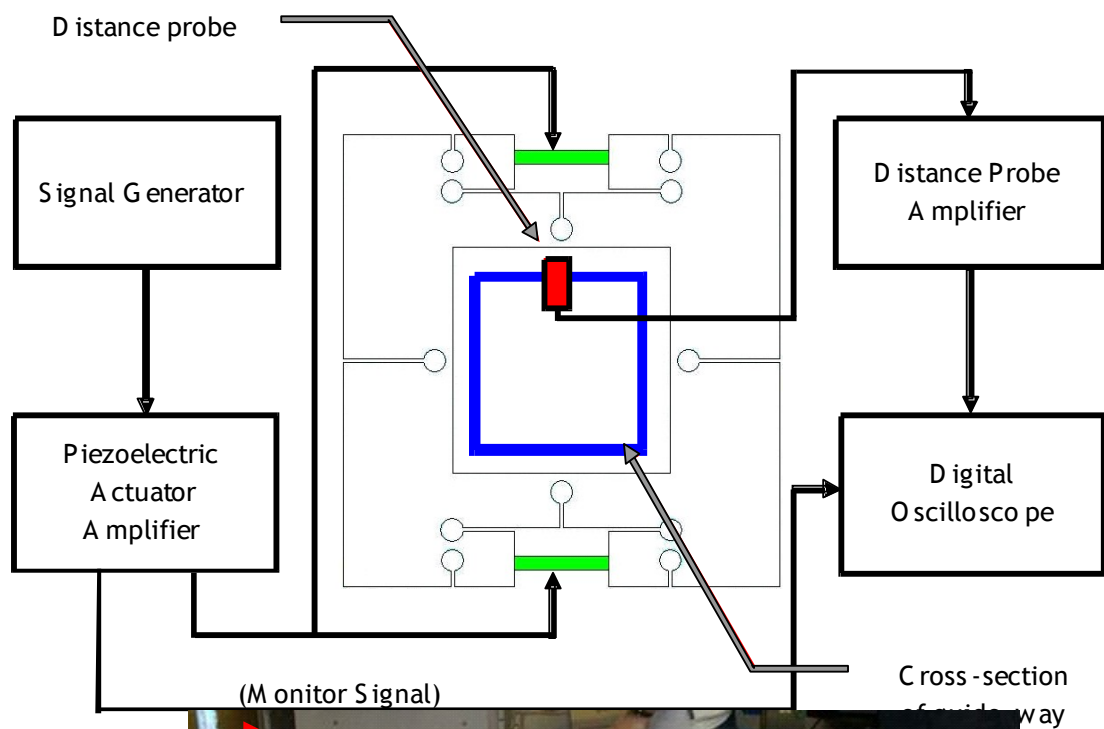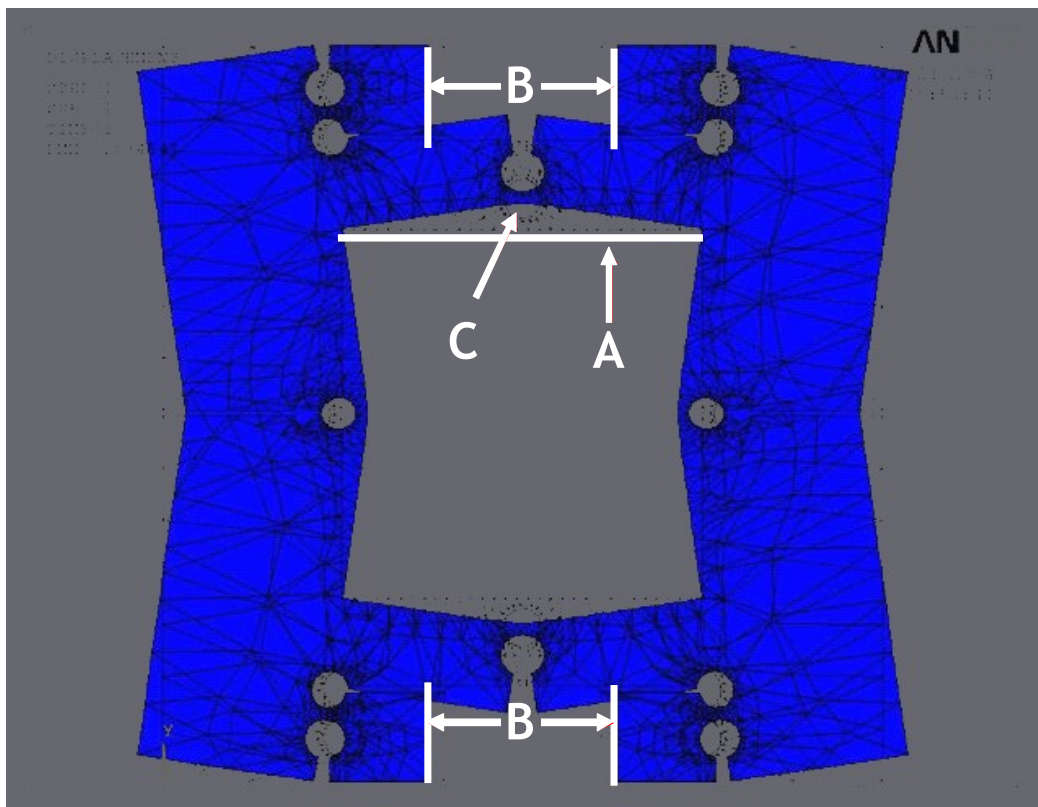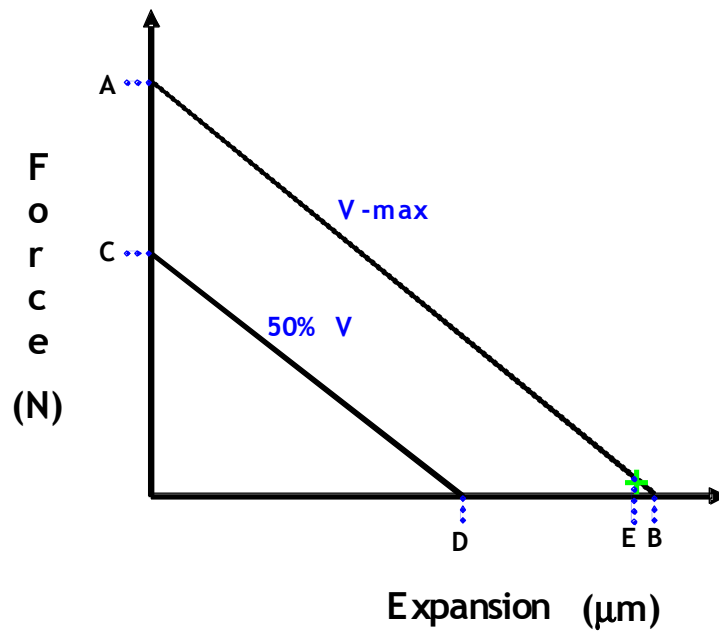
Figure 8

Figure 9

Figure 10
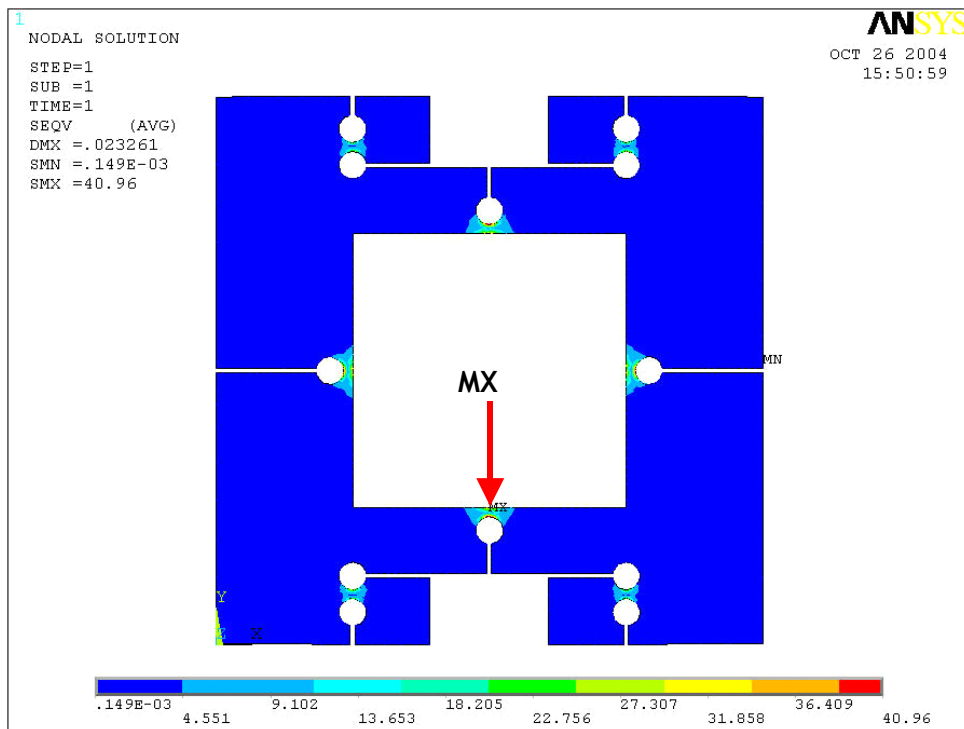
Figure 11
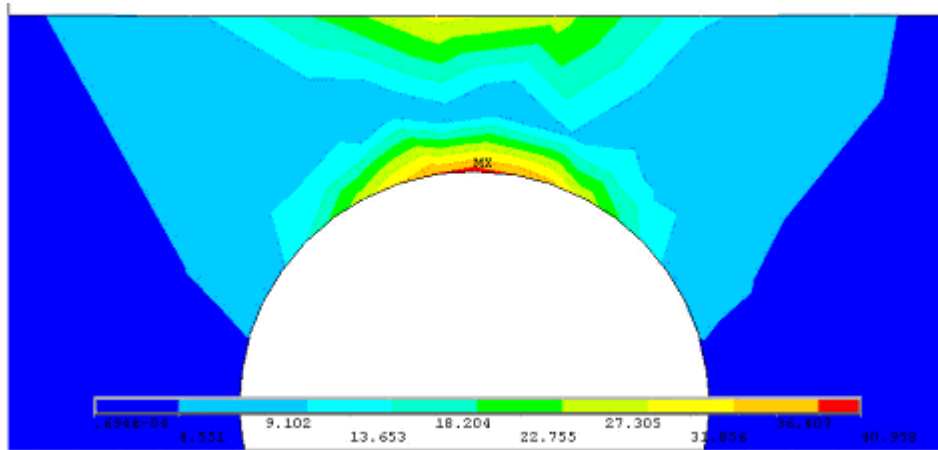
Figure 12

Figure 13

Figure 14

$$\frac{\partial P}{\partial Y} = 0$$

$$\frac{\partial H}{\partial Z} = 0$$

Air film under top surface of bearing

y

z

x
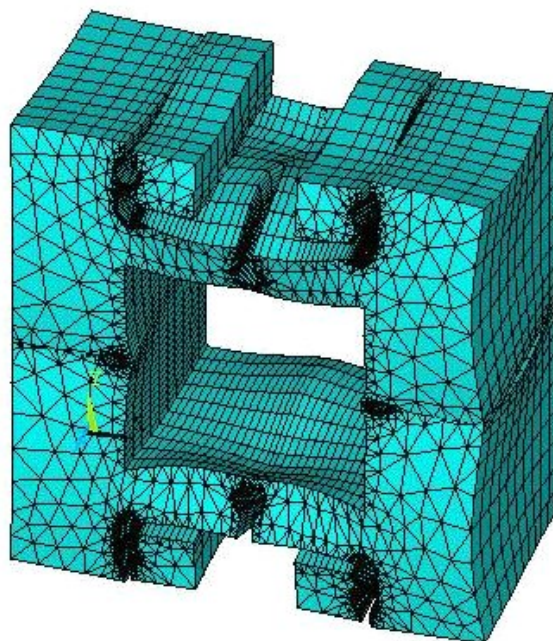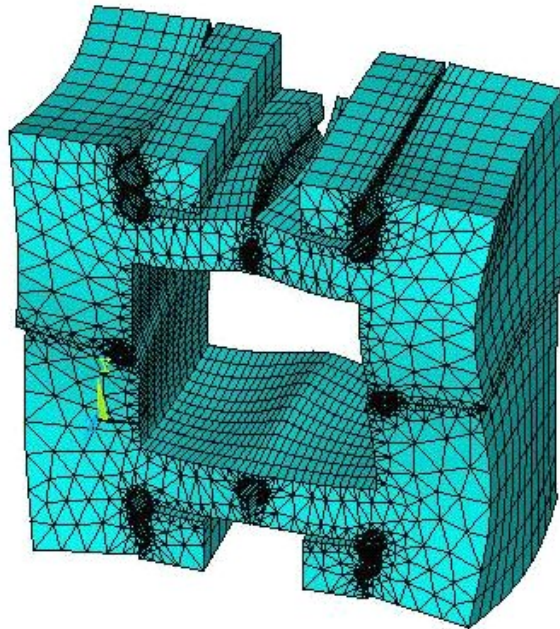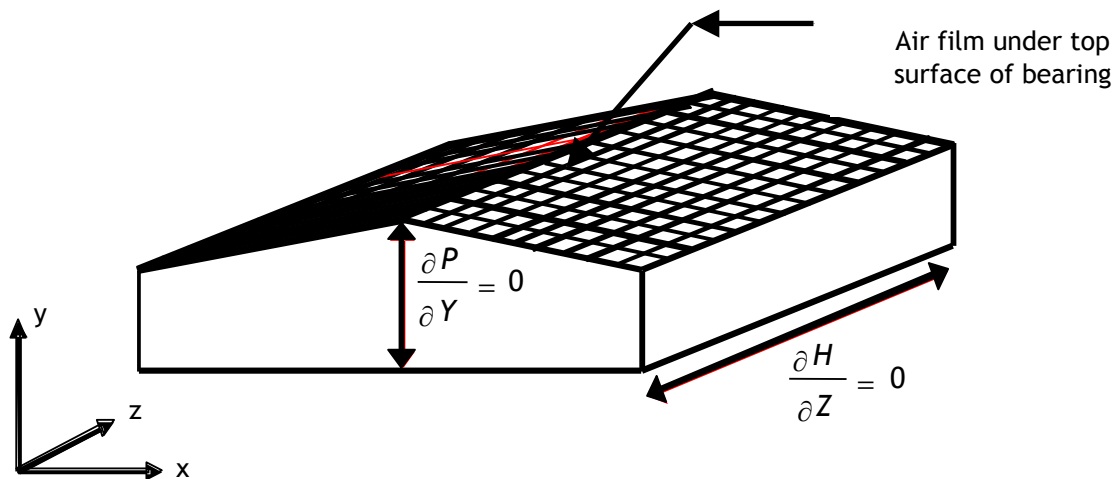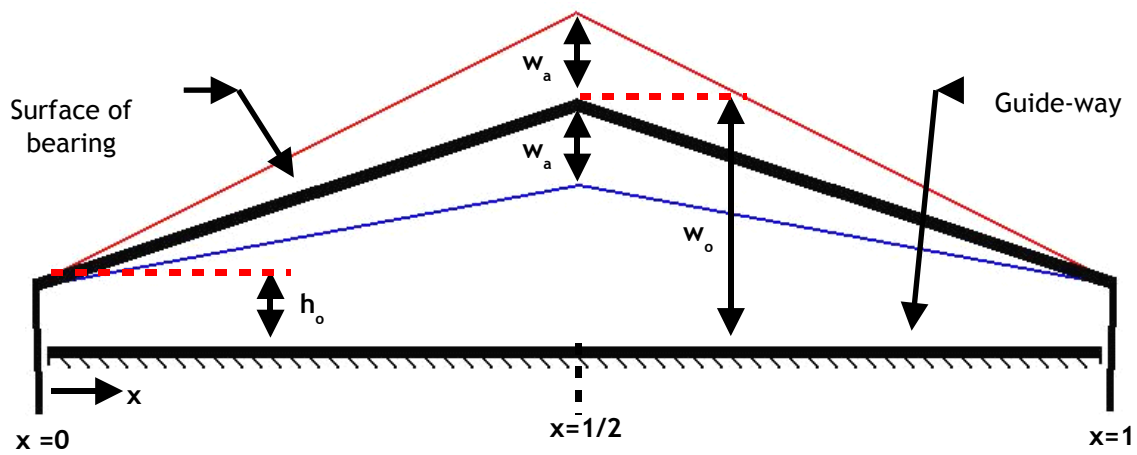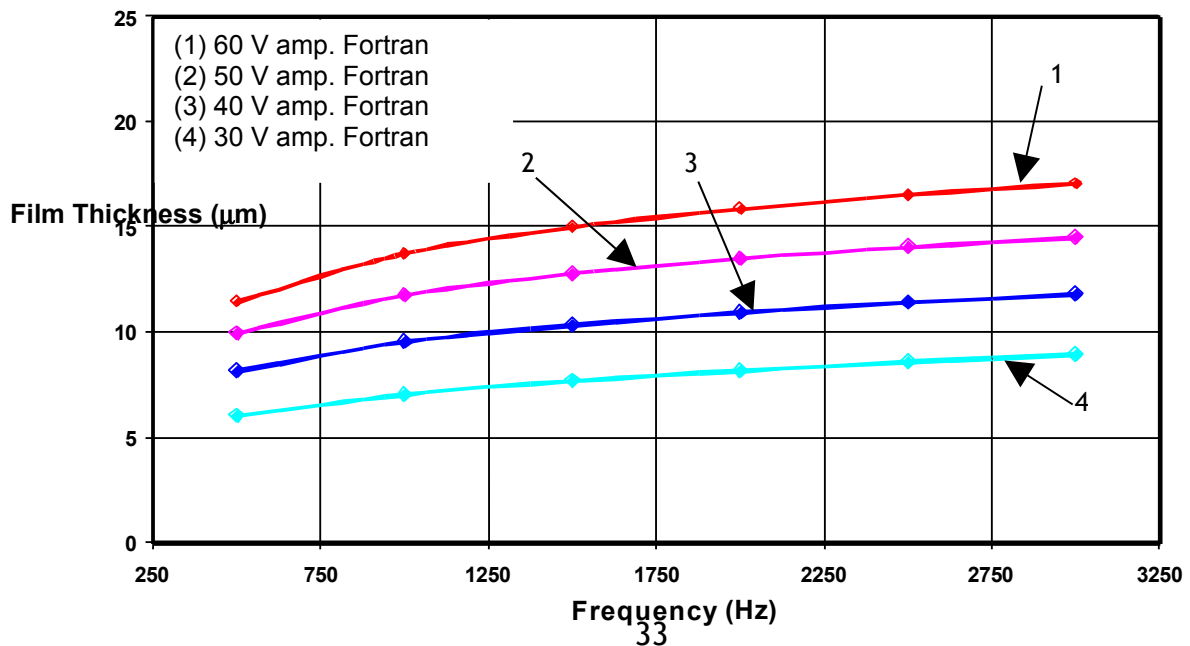
Figure 15

Figure 16

Figure 17
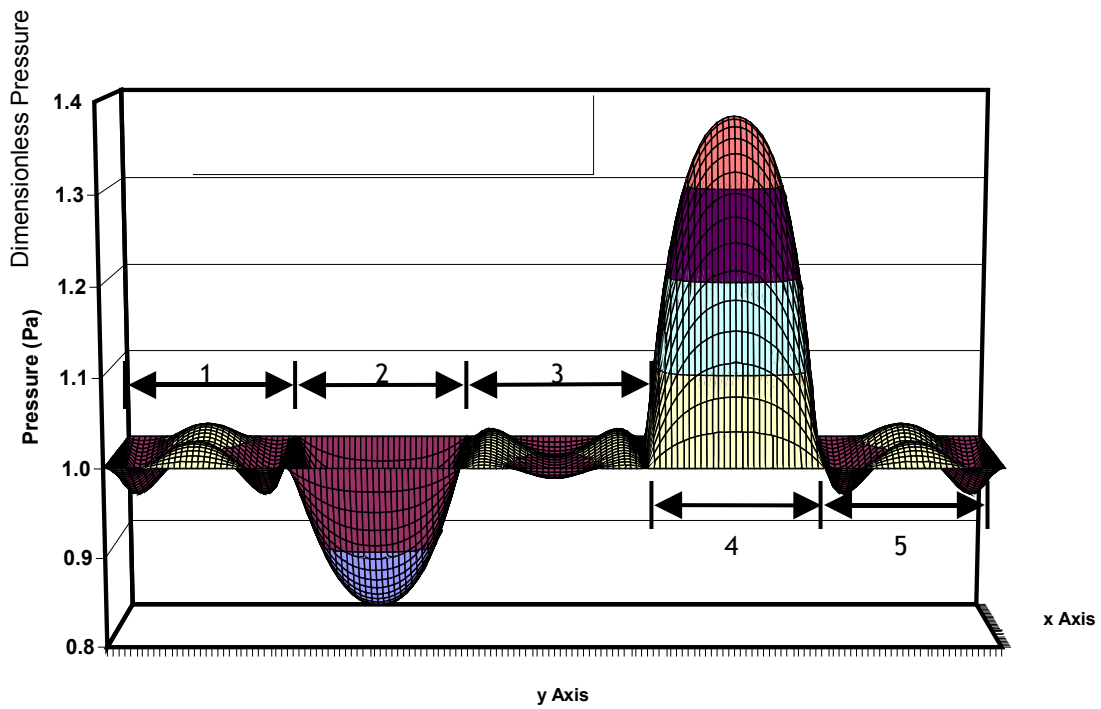
Figure 18

Figure 19

Figure 20

Figure 21

Figure 22

36

Figure 23

(1) Top surface increment
(2) Bottom surface increment
(3) Top surface decrement
(4) Bottom surface decrement
(5) FEA results
(6) Linear (FEA results)

Displacement (μm)

Off-set Voltage (V)

(1) 60 V input amplitude
(2) 60 V Fortran 2nd run
(3) 60 V Fortran amplitude

Figure 24

Film Thickness (μm)

37

Frequency (Hz)

Figure 25